Skyrme random-phase-approximation description of lowest $K^\pi = 2^+_\gamma$ states in axially deformed nuclei

V. O. Nesterenko,[1,*] V. G. Kartavenko,[1] W. Kleinig,[1,2] J. Kvasil,[3] A. Repko,[3] R. V. Jolos,[1] and P.-G. Reinhard[4]

[1]*Laboratory of Theoretical Physics, Joint Institute for Nuclear Research, Dubna, Moscow Region 141980, Russia*

[2]*Technische Universität Dresden, Institut für Analysis, D-01062 Dresden, Germany*

[3]*Institute of Particle and Nuclear Physics, Charles University, CZ-18000 Prague 8, Czech Republic*

[4]*Institut für Theoretische Physik II, Universität Erlangen, D-91058 Erlangen, Germany*

(Received 24 April 2015; revised manuscript received 19 January 2016; published 3 March 2016)

The lowest quadrupole γ-vibrational $K^\pi = 2^+$ states in axially deformed rare-earth (Nd, Sm, Gd, Dy, Er, Yb, Hf, W) and actinide (U) nuclei are systematically investigated within the separable random-phase-approximation (SRPA) based on the Skyrme functional. The energies E_γ and reduced transition probabilities $B(E2)$ of 2^+_γ states are calculated with the Skyrme forces SV-bas and SkM*. The energies of two-quasiparticle configurations forming the SRPA basis are corrected by using the pairing blocking effect. This results in a systematic downshift of E_γ by 0.3–0.5 MeV and thus in a better agreement with the experiment, especially in Sm, Gd, Dy, Hf, and W regions. For other isotopic chains, a noticeable overestimation of E_γ and too weak collectivity of 2^+_γ states still persist. It is shown that domains of nuclei with low and high 2^+_γ collectivity are related to the structure of the lowest two-quasiparticle states and conservation of the Nilsson selection rules. The description of 2^+_γ states with SV-bas and SkM* is similar in light rare-earth nuclei but deviates in heavier nuclei. However SV-bas much better reproduces the quadrupole deformation and energy of the isoscalar giant quadrupole resonance. The accuracy of SRPA is justified by comparison with exact RPA. The calculations suggest that a further development of the self-consistent calculation schemes is needed for a systematic satisfactory description of the 2^+_γ states.

DOI: 10.1103/PhysRevC.93.034301

I. INTRODUCTION

In recent decades, remarkable progress has been made in the description of nuclear dynamics within self-consistent mean-field (SCMF) models (Skyrme, Gogny, relativistic); see, e.g., the reviews [1–4]. In particular, a variety of quasiparticle random-phase-approximation (QRPA) methods were developed for the exploration of small-amplitude excitations in deformed nuclei, [5–15]. So far these methods have been used mainly for the description of giant resonances (GR) in light [6–9,11,13–15] and medium-heavy [5,9,12,14,16–19] nuclei. However, self-consistent QRPA was still rarely employed for the exploration of the lowest vibrational states (β, γ, octupole) in deformed rare-earth and actinide nuclei [10,12] (despite rich available experimental information for these regions [20,21]). This is partly due to the huge configuration spaces required for such deformed heavy nuclei. However, the main problem lies in a high sensitivity of the lowest vibrational states (LVS) to various factors. Following early calculations within the schematic quasiparticle-phonon model (QPM) [22–24], the description of LVS requires a proper treatment of the single-particle (s-p) spectra near the Fermi level, equilibrium deformation, pairing with the blocking effect, residual interaction (with both particle-hole and particle-particle channels), coupling to complex configurations (taking into account the Pauli principle), and exclusion of the spurious admixtures. Besides, the description of LVS should be consistent with the treatment of other collective modes, e.g., multipole GR. All these factors and requirements make the self-consistent description of LVS very demanding.

So far we are aware of two self-consistent QRPA studies of LVS in rare-earth and actinide regions: one with Gogny forces for ^{238}U [12] and another with Skyrme forces for rare-earth nuclei [10]. Actually only the latter study [10] is systematic. It covers γ-vibrational $K^\pi = 2^+_\gamma$ and β-vibrational $K^\pi = 0^+_\beta$ states in 27 rare-earth nuclei. The Skyrme forces SkM* [25] and SLy4 [26] are used, and performance of SkM* is found noticeably better than of SLy4. It is deduced that Skyrme QRPA is a reasonable basis for the investigation of LVS.

In the present paper, we continue the systematic exploration of 2^+_γ states in axial deformed nuclei with QRPA using Skyrme forces. The 2^+_γ states are chosen as the simplest case where we do not meet the problem of the extraction of the spurious admixtures. Compared to [10], our study has some important new aspects.

First, it is desirable to use for description of 2^+_γ states the Skyrme forces which simultaneously reproduce the energy of the isoscalar giant quadrupole resonance (ISGQR). Following [16], these forces should have a large isoscalar effective mass m^*_0/m. The forces from [10] have low effective masses, $m^*_0/m = 0.70$ for SLy4 [26] and 0.79 for SkM* [25], and so overestimate the ISGQR energy; see [16] and the discussion below. To make the description of ISGQR and 2^+_γ states consistent, we use in our calculations the recent SV-bas force [27] with $m^*_0/m = 0.9$. As shown below, SV-bas also manages to reproduce systematically well ground state deformations, a feature which is utterly crucial for a correct placing of LVS. Note that very similar results were earlier obtained [28] with the Skyrme force SV-mas10 [27] ($m^*_0/m = 1.0$). We choose here SV-bas as a more general parametrization which was already used in various studies, see, e.g., [4,18,19,29]. For comparison with [10], the force SkM* is also implemented.

*nester@theor.jinr.ru

Second, we take into account the pairing blocking effect (PBE) [22,30–33] which, following QPM studies [22–24], can be important for QRPA description of LVS in axially deformed nuclei. The PBE weakens the pairing and thus downshifts energies of low-energy two-quasiparticle (2qp) states by a few hundred keV [22–24], which in turn decreases the QRPA energies of 2^+_γ states. This effect can be especially important for slightly collective states (with one or two dominant 2qp components) which are often encountered among 2^+_γ states. We implement PBE within the Bardeen-Cooper-Schrieffer (BCS) scheme using volume pairing [34]. The same volume pairing, though in the framework of the Hartree-Fock-Bogoliubov (HFB) approach without PBE, was used in [10].

In fact, we are taking from the PBE only one aspect, namely the modification of 2qp energies. The 2qp states as such (s-p wave functions and pairing occupation amplitudes) remain untouched. This *ad hoc* solution to the problem with the energies of 2^+_γ states is admittedly not consistent. However, it has a great advantage of not disturbing the orthonormality of the 2qp basis, and thus it allows us to use the standard QRPA procedure. Following previous schematic [22–24] and our present studies, the PBE for 2^+_γ states in medium and heavy deformed nuclei can be strong and certainly deserves consideration. In this connection, our PBE-QRPA calculations can be viewed as a first step highlighting the problem and calling for further checking within a self-consistent PBE-QRPA prescription, yet to be developed.

The third new aspect is that we provide a detailed analysis of the obtained results, both numerically and analytically (e.g., in terms of simplified models for schematic RPA). We determine domains of nuclei with low and high collectivity of 2^+_γ-states and demonstrate that the lowest $K^\pi = 2^+$ 2qp state plays a key role in formation of these domains. The study embraces 9 isotopic chains (Nd, Sm, Gd, Dy, Er, Yb, Hf, W, U) with 41 axially deformed nuclei, as compared to 27 rare-earth nuclei in [10].

The calculations are performed within the separable random-phase-approximation (SRPA) method based on the Skyrme functional [1,35,36]. The method is developed in a one-dimensional (1D) version for spherical nuclei [37] and a two-dimensional (2D) version [5,38] for axial deformed nuclei. SRPA is derived self-consistently: (i) both the mean field and residual interaction are obtained from the same Skyrme functional, and (ii) the residual interaction includes all terms of the Skyrme functional as well as the Coulomb (direct and exchange) terms. The self-consistent factorization of the residual interaction dramatically reduces the computational effort for deformed nuclei while keeping high accuracy of the method. However SRPA is not self-consistent in the part of the pairing interaction because of (i) *ad hoc* implementation of the PBE into SRPA and (ii) skipping the particle-particle channel in the residual interaction.

In earlier studies, SRPA was successfully applied for the description of various GR in spherical and deformed nuclei: $E1(T = 1)$ and $E2(T = 0)$ [5,16,17,37], toroidal and compression $E1$ [18], and spin-flip $M1$ [19]. However, the success of the model for GR does not mean that it is also robust in the description of such fragile excitations as LVS. In this connection, we compare below some SRPA results with those obtained with the exact (not the separable ansatz) 2D QRPA code [39]. We find a nice agreement which confirms that SRPA is accurate enough.

The paper is organized as follows. In Sec. II the method and calculational details are outlined. The equations for the pairing blocking are given, the SRPA scheme is sketched, and SRPA results are compared with those from the exact QRPA. It is shown that SV-bas, unlike SkM*, nicely reproduces equilibrium quadrupole deformations and the ISQGR energy. Section III presents the main results for energies and reduced transition probabilities $B(E2)$ of 2^+_γ states. In Sec. IV, these results are discussed and analyzed in detail and compared with the previous data [10]. A summary is given in Sec. V. In Appendix A, the expression for the pairing matrix element is derived. In Appendix B, the basic SRPA equations are outlined. In Appendix C, a simple two-pole RPA model is presented, to be applied for explanation of the domains with low and high collectivity of 2^+_γ states. In Appendix D, SRPA strength constants of the residual interaction are compared with those of the QPM.

II. MODEL AND CALCULATION SCHEME

The SRPA approach [5] used in this paper is based on the Skyrme functional [1]

$$\mathcal{E}(\rho,\tau,\mathbf{J},\mathbf{j},\sigma,\mathbf{T}) = \mathcal{E}_{\rm kin} + \mathcal{E}_{\rm Sk} + \mathcal{E}_{\rm Coul} + \mathcal{E}_{\rm pair}, \qquad (1)$$

where $\mathcal{E}_{\rm kin}$ is the kinetic energy, $\mathcal{E}_{\rm Sk}$ is the potential energy according to the Skyrme functional, $\mathcal{E}_{\rm Coul}$ is the Coulomb energy, and $\mathcal{E}_{\rm pair}$ is the pairing energy. The Coulomb exchange term is treated in Slater approximation. The volume pairing corresponds to a zero-range pairing interaction. The Skyrme part $\mathcal{E}_{\rm Sk}$ depends on the local densities and currents: density $\rho(\mathbf{r})$, kinetic-energy density $\tau(\mathbf{r})$, spin-orbit density $\mathbf{J}(\mathbf{r})$, current $\mathbf{j}(\mathbf{r})$, spin density $\sigma(\mathbf{r})$, and spin-kinetic-energy density $\mathbf{T}(\mathbf{r})$ [1]. The mean-field Hamiltonian and SRPA residual interaction are self-consistently determined through the first and second functional derivatives of (1), respectively [5]. Further details of the model and calculation scheme are given below.

A. Mean field and quadrupole deformation

The stationary 2D mean-field calculations are performed with the SKYAX code [40] in cylindrical coordinates using a mesh size of 0.5 fm and a box size of about three nuclear radii. The single-particle space is chosen to embrace the levels from the bottom of the potential well up to energy 15–20 MeV. For SV-bas, the s-p schemes involve 304 proton and 375 neutron levels in ^{150}Nd and 379 proton and 485 neutron levels in ^{238}U.

The ground state is obtained by solving the mean-field equations and resides at the minimum of the total energy (1). Its axial quadrupole deformation is characterized by the dimensionless deformation parameter [41]

$$\beta_2 = \sqrt{\frac{5\pi}{3}}\frac{Q_2}{ZR^2}, \qquad (2)$$

where $Q_2 = \int d\mathbf{r}\rho_p(\mathbf{r})r^2Y_{20}$ is the quadrupole moment and $R = 1.2\,A^{1/3}$ fm, where A is the mass number.

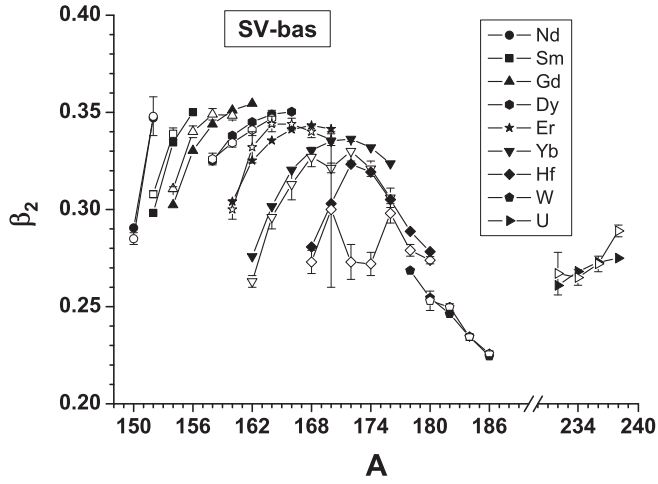

FIG. 1. Parameter β_2 of the axial quadrupole deformation in rare-earth and actinide nuclei. The values calculated with SV-bas [27] (full symbols) are compared with the experimental data [20] (open symbols with error bars).

Figure 1 compares deformation parameters calculated using SV-bas with available experimental data [20], and Fig. 2 shows the same comparison for SkM*. Figures 1 and 2 show very nice agreement for SV-bas while SkM* systematically overestimates β_2, especially in Yb, Hf, W, and U isotopes. Note that both SV-bas and SkM* fail to describe the particularly low values of experimental β_2 in ^{170}Yb and ^{172,174}Hf. Note also the exceptionally large error bars in ^{170}Hf.

B. Pairing and blocking effect

The volume pairing interaction reads

$$V^q_{\rm pair}(\mathbf{r},\mathbf{r}') = V_q\,\delta(\mathbf{r}-\mathbf{r}'), \tag{3}$$

where q stands for protons or neutrons and V_q are pairing strengths. In the present study pairing is treated at the BCS level [34].

If the pairing-blocking effect (PBE) is accounted for, the BCS problem is solved separately for the ground Ψ^q_0 and excited n-quasiparticle Ψ^q_n states. For the ground state, the expectation value $\langle\Psi^q_0|H_{\rm pair}|\Psi^q_0\rangle$ for the pairing Hamiltonian $H_{\rm pair}$ is minimized to determine the set of Bogoliubov coefficients $\{u^q_k, v^q_k\}$. For n-quasiparticle excitation, the wave function reads

$$\Psi^q_n = \hat\alpha^+_{j_1}\cdots\hat\alpha^+_{j_n}\Psi^q_0 = \hat a^+_{j_1}\cdots\hat a^+_{j_n} \times \prod_{k\neq j_1,\ldots,j_n\in q}\left[u^q_k(j_1,\ldots,j_n)+v^q_k(j_1,\ldots,j_n)\hat a^+_k\hat a^+_{\bar k}\right]|-\rangle, \tag{4}$$

where $\hat a^+_j(\hat\alpha^+_j)$ creates the particle (quasiparticle) at the state j and $|-\rangle$ is the particle vacuum. For this excitation, the expectation $\langle\Psi^q_n|H_{\rm pair}|\Psi^q_n\rangle$ is minimized and the new set of occupation numbers $\{u^q_k(j_1,\ldots,j_n), v^q_k(j_1,\ldots,j_n)\}$ specific for the given excitation is determined. In the latter case, the BCS equations for axially deformed nuclei (with doubly degenerate s-p levels) have a peculiarity: if some states from the set $\{j_1,\ldots,j_n\}$ are unpaired, then these states are excluded from the pairing scheme and contribute to the BCS equations as pure single-particle states. The physics behind this is obvious: if some level is occupied by an unpaired nucleon, then it is closed (i.e., blocked) for the pairing process which transfers nuclear pairs. This is so called the pairing blocking effect [22,30–33].

The PBE takes place in both BCS and HFB theories as soon as we deal with n-quasiparticle excitations. Most often the PBE is considered for 1qp excitations in odd and odd-odd nuclei; see, e.g., [29,34,42] and more references in [33]. Following QPM studies [22–24], the PBE may play a role in QRPA description of LVS in even-even axially deformed nuclei. Indeed 2qp states constitute the configuration space for QRPA. The first low-energy 2qp states are the main contributors to the lowest QRPA excitation. So it is worth checking how PBE for the low-energy 2qp states affects the description of LVS.

The main effect of the PBE is to change the 2qp energies [22–24]. Thus we use here, in an *ad hoc* manner, only one PBE output: PBE-corrected 2qp energies. Only they are implemented in SRPA, while the occupation amplitudes (u,v) and s-p wave functions are kept the same as in the BCS ground state. This has the advantage that orthonormality of the 2qp configuration space is maintained and the standard QRPA scheme remains applicable.

Usually in BCS+QRPA calculations the 2qp energies are computed by using the pairing gaps Δ_q, chemical potentials λ_q, and Bogoliubov coefficients $\{u^q_k, v^q_k\} \in q$ for the ground BCS state, yielding

$$\epsilon^q_{ij} = \epsilon^q_i + \epsilon^q_j, \tag{5}$$

where $\epsilon^q_i = \sqrt{(\tilde e^q_i - \lambda_q)^2 + \Delta^2_q}$ is the energy of the 1qp state and $\tilde e^q_i$ is the renormalized s-p energy (see the expression below). In HFB+QRPA calculations, the 2qp states for the QRPA configuration space are also expressed in terms of ground state values. In particular, their energies are calculated as a sum of two 1qp energies in the canonical basis using the HFB solutions for the ground state; see, e.g., [9,10,12]. So both the BCS and HFB schemes usually omit the PBE for the 2qp states. Following QPM and our calculations, such a treatment can be insufficient for a correct description of the LVS.

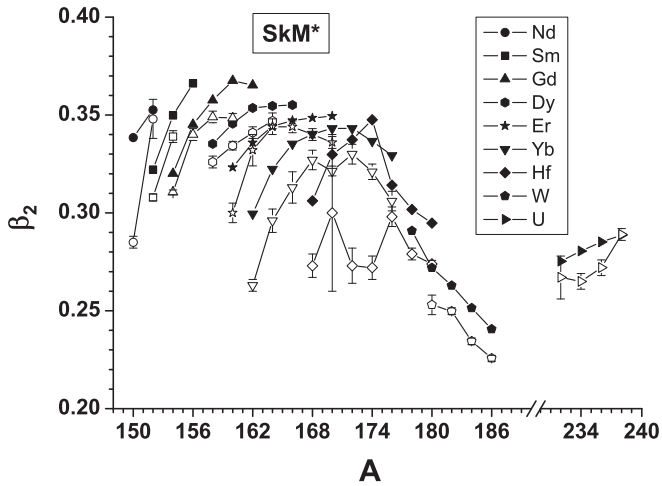

FIG. 2. The same as Fig. 1 but for SkM*.

For $K^\pi = 2^+$ states,

$$\Psi^q(ij) = \hat{\alpha}_i^+ \hat{\alpha}_j^+ \Psi_0^q = \hat{a}_i^+ \hat{a}_j^+ \prod_{k\neq i,\, j\in q} \left(u_k^q(ij) + v_k^q(ij)\hat{a}_k^+ \hat{a}_{\bar{k}}^+\right)|-\rangle, \quad (6)$$

the 2qp pairs are necessarily nondiagonal ($i \neq j$). For a *constant* pairing force, the BCS-PBE prescription for this case was formulated in [22]. Below we present the BCS-PBE formalism for the δ-force volume pairing (3). For each 2qp state $\Psi^q(ij)$, one should solve the system of BCS+PBE equations

$$\left[u_k^q(ij)\right]^2 = \frac{1}{2}\left\{1 + \frac{\tilde{e}_k^q - \lambda_q(ij)}{\sqrt{\left[\tilde{e}_k^q - \lambda_q(ij)\right]^2 + \left[\Delta_k^q(ij)\right]^2}}\right\}, \quad (7)$$

$$\left[v_k^q(ij)\right]^2 = \frac{1}{2}\left\{1 - \frac{\tilde{e}_k^q - \lambda_q(ij)}{\sqrt{\left[\tilde{e}_k^q - \lambda_q(ij)\right]^2 + \left[\Delta_k^q(ij)\right]^2}}\right\}, \quad (8)$$

$$\Delta_k^q(ij) = -\sum_{k'\neq i,\, j}^{K'>0,k'\in q} f_{k'}^q V_{k\bar{k}k'\bar{k}'}^{(\mathrm{pair,q})}\, v_{k'}^q(ij) u_{k'}^q(ij), \quad (9)$$

$$N_q = 2 + \sum_{k'\neq i,\, j}^{K'>0,k'\in q} f_{k'}^q \times \left\{1 - \frac{\tilde{e}_k^q - \lambda_q(ij)}{\sqrt{\left[\tilde{e}_k^q - \lambda_q(ij)\right]^2 + \left[\Delta_k^q(ij)\right]^2}}\right\}, \quad (10)$$

where

$$\tilde{e}_k^q = e_k^q - 1/2 \sum_{k'\in q} f_{k'}^q V_{k\bar{k}k'\bar{k}'}^{(\mathrm{pair,q})} \left[v_k^q\right]^2 \quad (11)$$

is the renormalized s-p energy and e_k^q is the initial s-p energy. Furthermore, $u_k^q(ij), v_k^q(ij), \Delta_k^q(ij), \lambda_q(ij)$ are Bogoliubov coefficients, pairing gaps, and chemical potentials, calculated for the 2qp (ij) excitation. The sums in (9) and (10) include all s-p states k' (with isospin q and projection $K' > 0$ of the total angular momentum) with the exception of $k' = i$ and j; $N_p = Z$ and $N_n = N$ are proton and neutron numbers. The smoothing energy-dependent cutoff weights $f_{k'}^q$ are introduced to cure the well-known drawback of the zero-range pairing force to overestimate the coupling to the (continuum) high-energy states [31,33]. Expressions for weights $f_{k'}^q$ and pairing matrix elements $V_{k\bar{k}k'\bar{k}'}^{(\mathrm{pair,q})}$ in axial nuclei are given in Appendix A.

The PBE-corrected energy of the 2qp excitation reads

$$\mathcal{E}_{\mathrm{bl}}^q(ij) = \mathcal{E}^q(ij) - \mathcal{E}_0^q, \quad (12)$$

where

$$\mathcal{E}_{\mathrm{bl}}^q(ij) = \langle\Psi^q(ij)|H_{\mathrm{pair}}^q|\Psi^q(ij)\rangle = \tilde{e}_i^q + \tilde{e}_j^q + \sum_{k\neq i,\, j}^{K>0,k\in q} f_k^q\left[2\tilde{e}_k^q\left(v_k^q(ij)\right)^2 - \Delta_k^{(q)}(ij) u_k^q(ij) v_k^q(ij)\right] \quad (13)$$

is the energy of the q subsystem in the (ij) state and

$$\mathcal{E}_0^q = \left\langle\Psi_0^q\middle|H_{\mathrm{pair}}^q\middle|\Psi_0^q\right\rangle = 2\sum_k^{K>0,k\in q} f_k^q \tilde{e}_k^q \left(v_k^q\right)^2 - \sum_k^{K>0,k\in q} f_k^q \Delta_k^q\, u_k^q\, v_k^q \quad (14)$$

is the energy of the q subsystem in the ground state. The values $u_k^q, v_k^q, \Delta_k^q, \lambda_q$ in (14) are for the ground state. Equations (9), (10), and (13) show that PBE excludes the states i and j from the pairing sums. These blocked states do not contribute to the pairing gap (9) and enter (10) and (13) as single-particle (not quasiparticle) states.

The sums in (9), (10), and (13) are usually dominated by a few k' states around the Fermi level. If the states i and j belong to this group, then their blocking can effectively decrease the level density near the Fermi level and thus the pairing gap (9). Consequently the energy (13) is changed. In such cases, the pairing is significantly suppressed and the BCS-PBE value for the 2qp energy (12) becomes a few hundred keV smaller than the BCS energy (5) [22]. This in turn leads to a significant downshift of the energy of the first QRPA solution.

In the present study, we block the five lowest $K^\pi = 2^+$ 2qp states (proton and neutron altogether). The calculations show that this number of blocked states is optimal. More blocking would involve the states that are remote by energy from the Fermi level and thus have a negligible PBE. Less blocking is likely to miss a part of the PBE corrections.

We substitute the PBE-corrected energies $\mathcal{E}_{\mathrm{bl}}^q(ij)$ to SRPA replacing the ϵ_{ij}^q. However, we do not use the PBE-modified Bogoliubov coefficients $\{u_k^q(ij), v_k^q(ij)\}$. Instead we continue to employ in SRPA the ground state set $\{u_k^q, v_k^q\}$ and wave functions. This leaves the 2qp basis orthonormalized and renders our PBE-SRPA scheme easily applicable.

It is also worthwhile to inspect a possible impact of our scheme on the basic features of QRPA, namely stability of the QRPA interaction matrix, elimination of spurious modes, and sum rules. (i) Concerning the QRPA matrix, the PBE-induced reduction of the positive diagonal elements (2qp energies) of the matrix indeed can cause instabilities in some cases. This is checked numerically. We find that for the $K^\pi = 2^+$ states studied here the QRPA remains in the stable regime. The only exception is ^{164}Dy in the calculations with the force SkM*; see the discussion below. (ii) Spurious modes must be carefully checked when trying to apply the PBE to other quadrupole states, say with $K^\pi = 0^+$ and $K^\pi = 1^+$, but not in our case. For $K^\pi = 2^+$ states the spurious modes are absent. (iii) Concerning the sum rules, there is some quantitative effect. But it is extremely small, as the main contribution to sum rules comes from higher lying states which are not affected by the PBE. Altogether, the present *ad hoc* implementation of the PBE looks robust. It still calls for a thorough formal self-consistent development which, however, will be tedious and take time. We consider the present study as a first step in exploration of the impact of the PBE on low-lying spectra of $K^\pi = 2^+$ states.

The PBE should be applied with care in case of a weak pairing, because the blocking reduces pairing and may trigger its full breakdown. In the worst case, a more involved

formalism (allowing a weak pairing) should be used, e.g., the method with particle-number projection before variation [43]. Calculations with this method show that BCS-PBE somewhat underestimates the 2qp energies [43]. However, the projection method requires a huge effort, and it cannot be consistently applied for the Skyrme energy functional [44]. So we use here BCS-PBE, though staying alert for suspect cases.

C. SRPA scheme

The SRPA formalism for axial nuclei is described in detail elsewhere [5,38]. Here we sketch only the points relevant for the present study. As mentioned above, the SRPA formalism starts from the functional (1). The residual interaction includes contributions from both time-even and time-odd densities and also takes care of the Coulomb interaction. The coupling between the quadrupole $\lambda\mu = 22$ and hexadecapole $\lambda\mu = 42$ modes, pertinent to deformed nuclei, is included. The basic SRPA equations and more calculation details can be found in Appendix B.

The present SRPA version skips the particle-particle (hole-hole) channel for $K^\pi = 2^+$ states. In QPM the pp channel is used to harmonize description of LVS energies and transition probabilities [24] but these calculations are not self-consistent. The self-consistent Skyrme BCS-QRPA calculations for spherical nuclei show that the pp channel tends to decrease the LVS energies [46]. If so, then this effect can be partly compensated by the energy upshift gained by using the particle-projection method [43]. The Skyrme HFB-QRPA studies of LVS in deformed nuclei use the pp channel only partly [10] if at all [9]. In general, the pp channel, being crucial for β-vibrational $K^\pi = 0^+$ states, seems not to be so important for γ-vibrational $K^\pi = 2^+$ states. At least we do not know of any self-consistent study for the lowest $K^\pi = 2^+$ states in axial deformed nuclei, which would demonstrate a real need for this channel.

In the present study, we calculate the structure and energies of the first RPA one-phonon 2^+_γ states ($\lambda\mu\nu = 221$) in Nd, Sm, Gd, Dy, Er, Yb, Hf, W, and U isotopes. The reduced probability $B(E2) = |\langle \nu = 1| \sum_{k=1}^{Z} r_k^2 Y_{22}(\theta_k)|0\rangle|^2$ of the transition from the ground $|0\rangle$ to the SRPA $\nu = 1$ state is also computed.

The configuration space for $\lambda\mu = 22$ involves, depending on the isotope, 6600–9600 proton and 9400–14 200 neutron 2qp states with excitation energies up to 55–80 MeV. This basis is sufficient for our aims. It results (together with the quadrupole components $\lambda\mu = 20$ and 21) in a reasonable exhaustion of the total energy-weighted sum rule $\mathrm{EWSR}(E2, T = 0) = (\hbar^2 e^2)/(8\pi m_p) 50 A \langle r^2 \rangle_A$ by ∼95–98%. A similar size of configuration space was used in [10] and [12] (19 000–28 000 and 23 000–26 000 2qp states, respectively).

The calculations are performed for the Skyrme parametrizations SV-bas and SkM*. As mentioned in the Introduction, SV-bas is chosen because it provides an accurate description of the ground state deformations and ISGQR energies. The latter is demonstrated in Fig. 3, where ISGQR strength functions and energy centroids (see definitions in Appendix B) are depicted for SV-bas and SkM*. The calculated centroids are 12.2 and 13.0 MeV in ^{152}Nd, 12.0 and 12.5 MeV in ^{164}Dy, 11.8 and 12.3 MeV in ^{172}Yb, and 10.7 and 11.1 MeV in ^{238}U, for SV-bas and SkM* respectively. These results are compared

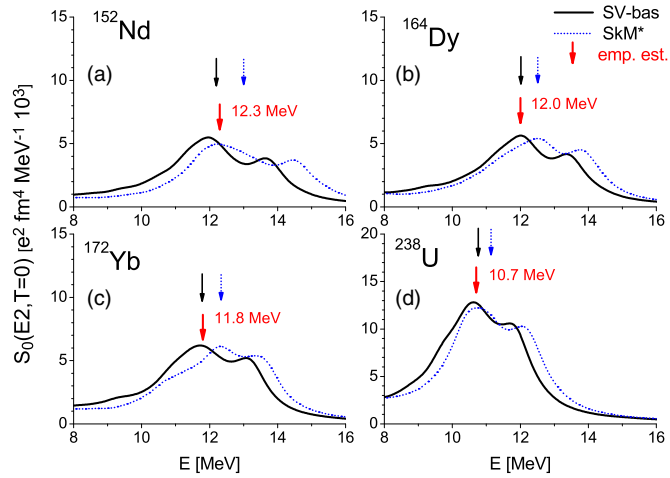

FIG. 3. The isoscalar strength function for the ISGQR in ^{152}Nd, ^{164}Dy, ^{172}Yb, and ^{238}U, calculated with the Skyrme forces SkM* [25] (dotted blue line) and SV-bas [27] (solid black line). The Lorentz averaging parameter is $\Delta = 1$ MeV. The empirical estimates for the ISGQR centroids [45] are marked by lower red arrows with indicated energies. The SV-bas and SkM* estimates for the centroids are denoted by upper black solid and blue dotted arrows, respectively.

with the empirical polynomial estimations [45]. It is seen that SV-bas well describes the energy centroids while SkM* systematically overestimates them. So SV-bas demonstrates a good reproduction of both axial deformations and ISGQR energies, which makes SV-bas a promising candidate for the description of γ-vibrational states.

To demonstrate the accuracy of SRPA, we compare in Fig. 4 some results for $K^\pi = 2^+_\gamma$ states obtained within SRPA and exact 2D QRPA [39]. The exact method is noted as eRPA. In both cases, the calculations are performed without PBE and pp channel in the residual interaction. The isotopic chains with

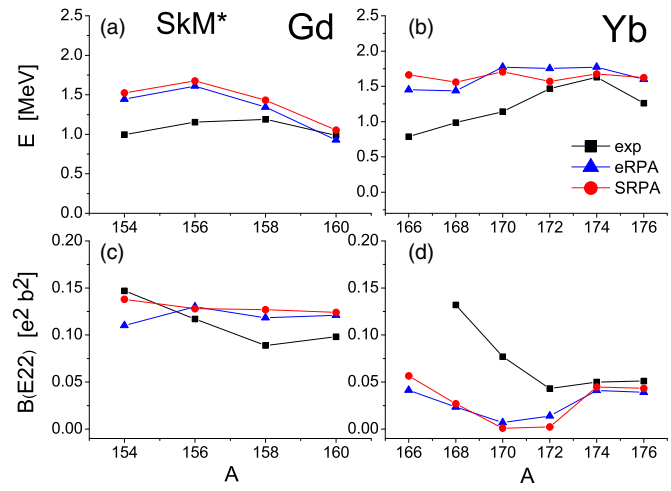

FIG. 4. Energies [(a) and (b)] and $B(E2)$ values [(c) and (d)] of the 2^+_γ-vibrational states, calculated with the force SkM* in the framework of SRPA (red circles) and exact eRPA (blue triangles) in Gd (left) and Yb (right) isotopes. In both calculations, the PBE and pp channel in the residual interaction are omitted. The experimental data [20] are depicted by black squares.

high (Gd) and low (Yb) collectivity of 2^+_γ states are considered. We see a very nice agreement between SRPA and eRPA results, which demonstrates the robustness of SRPA. Since SRPA calculations require much less computational effort than eRPA, just SRPA is used in the following.

III. MAIN RESULTS

A. Main results

Results of our calculations for the lowest 2qp states, SRPA energies, and $B(E2)$ values of 2^+_γ states are presented in Figs. 5–10. Cases without and with PBE are considered, using for 2qp energies Eqs. (5) and (12), respectively. The results are compared with available experimental data [20]. Note that experimental errors for 2^+_γ energies are typically ± 0.01 MeV, i.e., much smaller than the relevant values to be discussed. Concerning $B(E2)$, the errors usually do not exceed 10% for collective states ($B(E2) > 0.1$–$0.09\ e^2\mathrm{b}^2$) but can reach 15–30% in less collective states (^{150}Nd, ^{154}Sm, $^{170-176}$Yb, ^{238}U). In the figures for SkM*, results are compared with those of [10] (manually extracted from the figures of that paper).

Figure 5 shows the results for Nd, Sm, and Gd isotopes obtained with SV-bas. Calculations without PBE [plots (a)–(c)] essentially overestimate the 2^+_γ energies. The discrepancy decreases from Nd to Gd with the growth of the collective shift $\Delta E = \mathcal{E}_{2\mathrm{qp}} - E_{\mathrm{SRPA}}$ (the difference between the lowest 2qp and SRPA energies). It is seen that the PBE noticeably downshifts the 2qp energies and thus the SRPA energies [plots (d)–(f)]. The downshift reaches 0.1–0.6 MeV, depending on the isotope. As a result, the agreement with experimental energies improves, especially in heavy Gd isotopes. The trends of E_{SRPA} with mass number A are approximately reproduced. The $B(E2)$ values in Sm and Gd with and without blocking are about the same. In Nd isotopes, the calculated 2^+_γ states demonstrate a weak collectivity, i.e., low $B(E2)$ values. Here the PBE worsens the agreement. The SkM* results in Fig. 6 for the same isotopes provide a similar quality of description. SRPA calculations without PBE agree well with HFB-QRPA ones [10], which indicates again the accuracy of our method.

Figure 7 shows the SV-bas results for Dy, Er, and Yb isotopes. The collectivity of calculated 2^+_γ states reaches a maximum in Dy and Er isotopes. Here we have the largest ΔE and $B(E2)$. The collectivity starts to decrease in heavy Er isotopes and almost vanishes in Yb. The PBE considerably decreases the 2qp and SRPA energies. In Dy isotopes, this leads to a nice agreement with the experimental energies. In Er and Yb, the PBE noticeably improves the description of 2^+_γ energies. However, E_{SRPA} still remain considerably higher than E_{exp} and calculated $B(E2)$ are accordingly underestimated.

The SkM* results for Dy-Er-Yb isotopes are given in Fig. 8. We again observe a decrease of collectivity of 2^+_γ states from Dy to Yb isotopes. However, unlike the case of light rare-earth nuclei in Figs. 5 and 6, we also see a significant difference in the results of SV-bas and SkM*. First, as compared to SV-bas results and experimental data, the SkM* energies in Er and Yb isotopes strongly fluctuate with A, closely following variations of 2qp energies (this feature of SkM* results was also mentioned in [10]). Such fluctuations point to a small collectivity of 2^+_γ states and significant contribution of the lowest 2qp state to the structure of 2^+_γ state. Furthermore, the 2qp energies are generally smaller for SkM* than for SV-bas, which results in a better average description of E_{exp} in Er and Yb with SkM*. The PBE gives here larger changes than for Nd-Sm-Gd isotopes. In particular, it leads to a huge decrease of 2^+_γ energy in ^{164}Dy (like in [10]). This state becomes extremely collective (see a huge overestimation of experimental $B(E2)$). It is unlikely that it can be described within a familiar QRPA and needs a more involved prescription taking into account large ground state correlations [47–49]. The SRPA results agree with HFB-QRPA ones [10] for Er and Yb but not for Dy, especially in the exceptional case of ^{164}Dy.

Figures 9 and 10 show the results for heavy rare-earth Hf and W isotopes and for actinide U isotopes. For both forces, the collectivity of 2^+_γ states increases from Hf to W and decreases in U. Moreover, both forces give rather similar trends of E_{SRPA} with A, though deviating from the experimental ones. The PBE considerably downshifts the 2qp and SRPA energies and thus in general improves their description. On average, SkM* energies are closer to E_{exp} than SV-bas ones but give more fuzzy A dependence, especially with PBE. In U isotopes, the description of the spectra with SkM* is much better than with SV-bas, which again is explained by lower 2qp energies in SkM*. The description of $B(E2)$ is acceptable in heavy Hf isotopes for both SV-bas and SkM*. With exception of ^{184}W, the PBE does not affect the description of $B(E2)$.

Altogether, the results from Figs. 5–10 allow us to draw the following conclusions: (i) In rare-earth and actinide regions, there are pronounced isotopic domains with low and high collectivity of 2^+_γ states. (ii) The best agreement with the experimental data is obtained for Dy (except for ^{164}Dy) and W isotopes, i.e., for the most collective 2^+_γ states characterized by large ΔE and $B(E2)$ values. (iii) The PBE essentially downshifts 2qp and SRPA energies, thus leading to a better agreement with experiment. The value of the downshift is comparable with the collective shift ΔE of SRPA and is much larger than the experimental errors [20]. This indicates that the PBE plays a non-negligible role for energies of low lying states. At the same time, the blocking has only a small effect on the $B(E2)$ values. Note that the results (iii) should be checked within a truly self-consistent PBE-QRPA approach, yet to be developed.

The above conclusions are supported by both SV-bas and SkM*. These two forces give similar results in light rare-earth nuclei but deviate in heavier nuclei. In SV-bas, the E_{SRPA} vary less with system size A but are usually larger than E_{exp}. In SkM*, the variation of E_{SRPA} is stronger, but this force gives lower 2qp and SRPA energies and thus better describes E_{exp}, e.g., in U isotopes. The differences are partly caused by a weaker pairing in SkM* (the gaps in SkM* are on average 30–50% smaller than in SV-bas). The latter in turn can follow from different level densities of SV-bas and SkM* s-p spectra.

It is also useful to inspect the r.m.s. deviations of the calculated results from the experimental data,

$$\sigma_b = \sqrt{\frac{\sum_{i=1}^{\mathcal{N}_b} \left(b_i^{\mathrm{cal}} - b_i^{\mathrm{exp}}\right)^2}{\mathcal{N}_b}}, \tag{15}$$

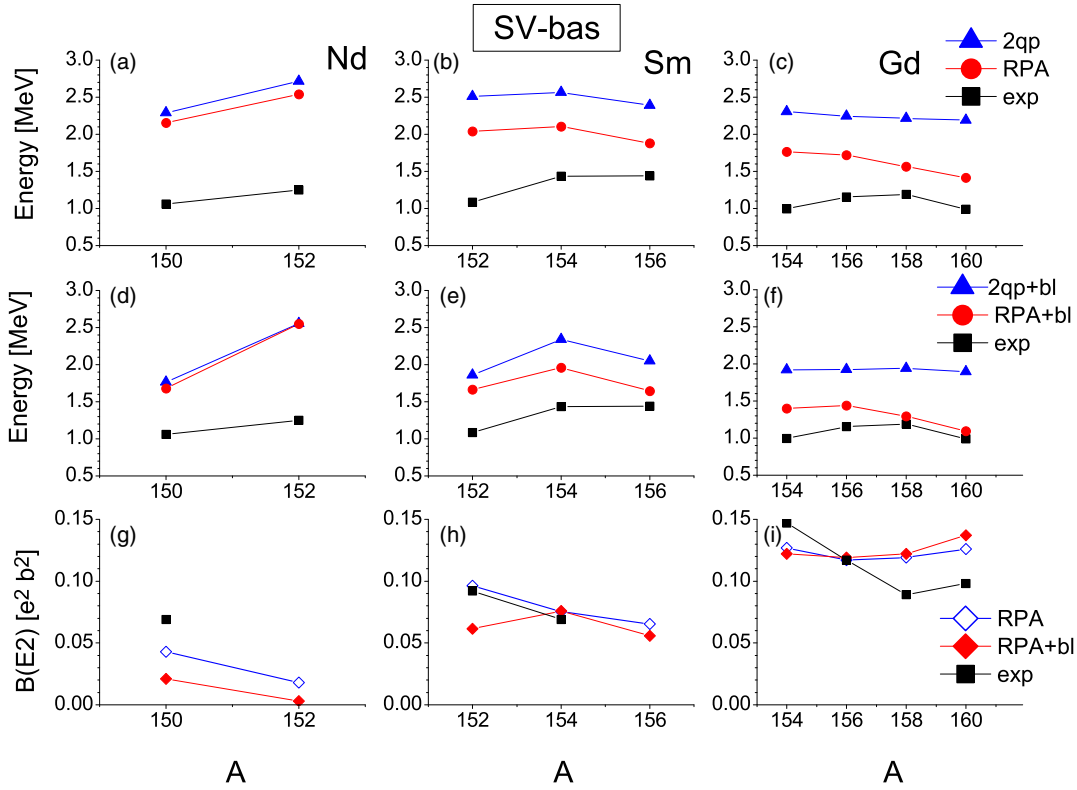

FIG. 5. The lowest 2qp and SRPA (marked as RPA) energies [(a)–(f)] as well as $B(E2)$ values [(g)–(i)] of 2^+_γ-vibrational states in Nd (left), Sm (center), and Gd (right) isotopes, calculated with the force SV-bas. The 2qp (filled blue triangles) and SRPA (filled red circles) energies are obtained without [(a)–(c)] and with [(d)–(f)] PBE. The SRPA $B(E2)$ values without (empty blue diamonds) and with (filled red diamonds) PBE are plotted in (g)–(i). In all the plots, the experimental data [20] are given (filled black squares).

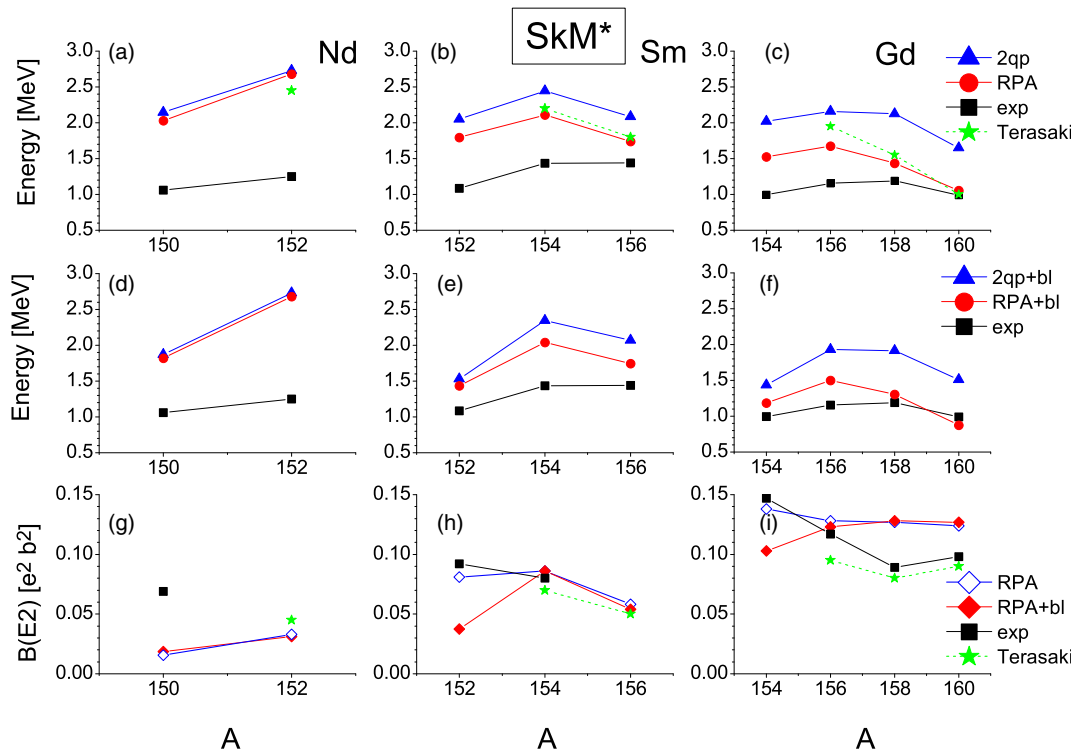

FIG. 6. The same as in Fig. 5 but for SkM*. For comparison, the SkM* results [10] are depicted (filled green stars).

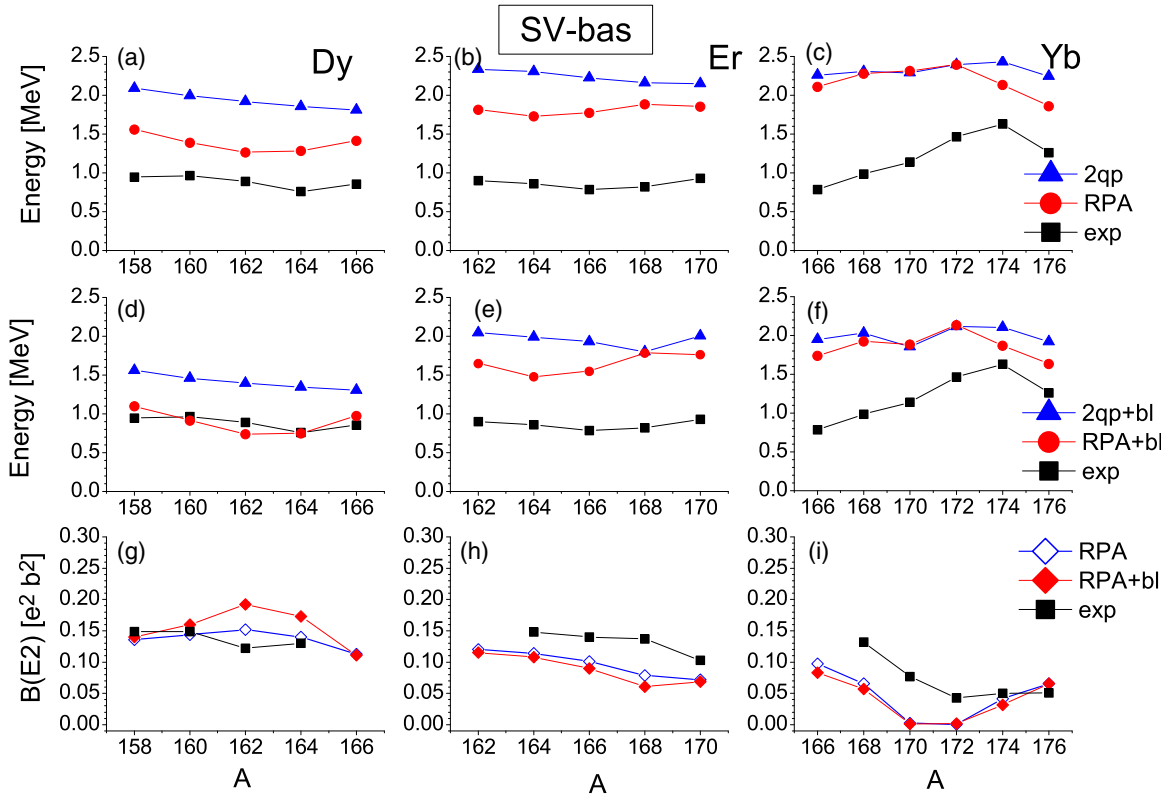

FIG. 7. The SV-bas results as in Fig. 5 but for Dy, Er, and Yb isotopes.

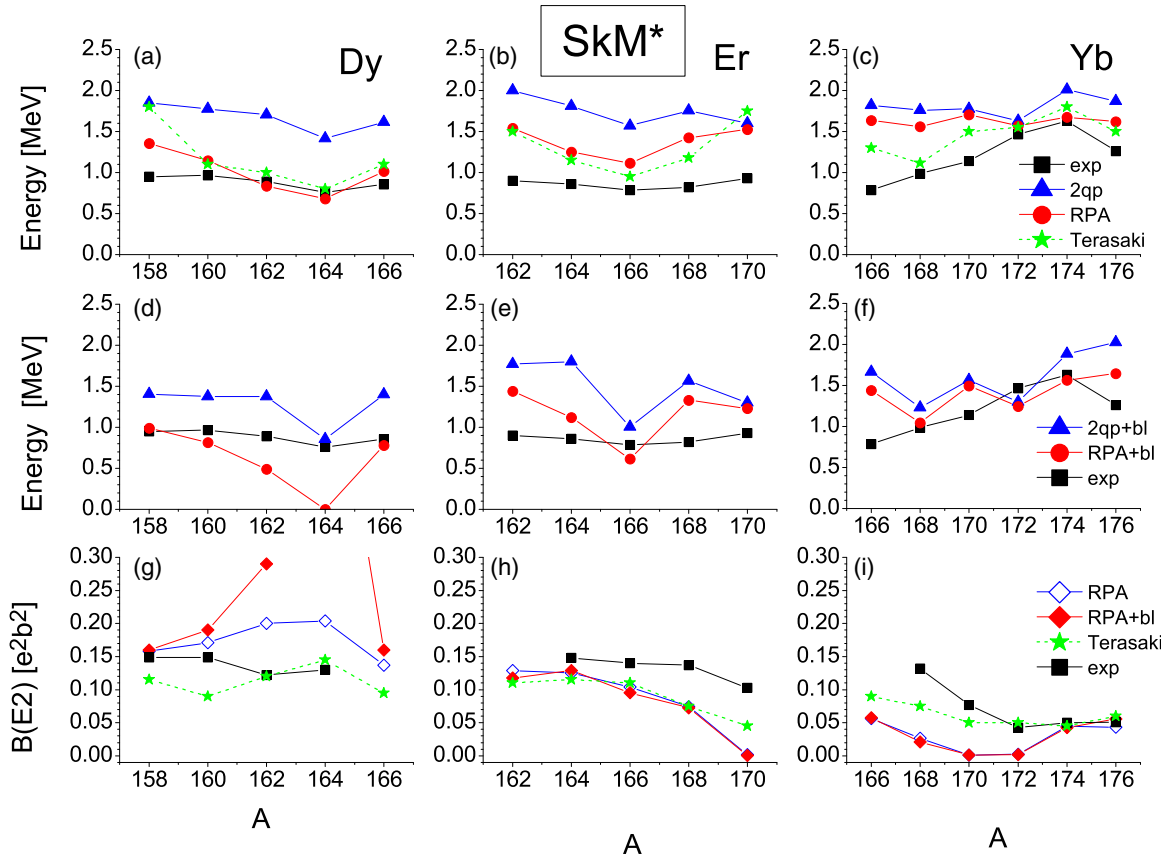

FIG. 8. The same as in Fig. 6 but for SkM*. In the plot (g), the $B(E2) = 0.7\ e^2\mathrm{b}^2$ for ^{164}Dy is beyond the exhibited interval.

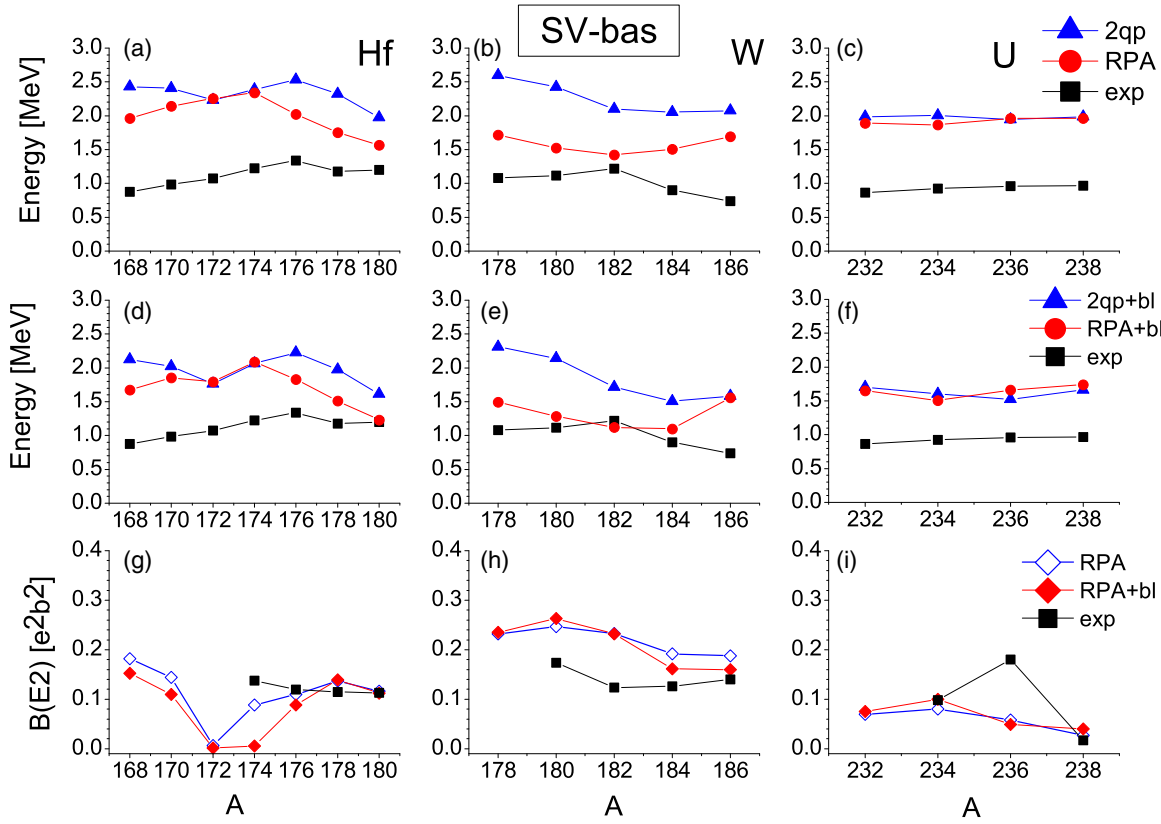

FIG. 9. The SV-bas results as in Fig. 7 but for Hf, W, and U isotopes.

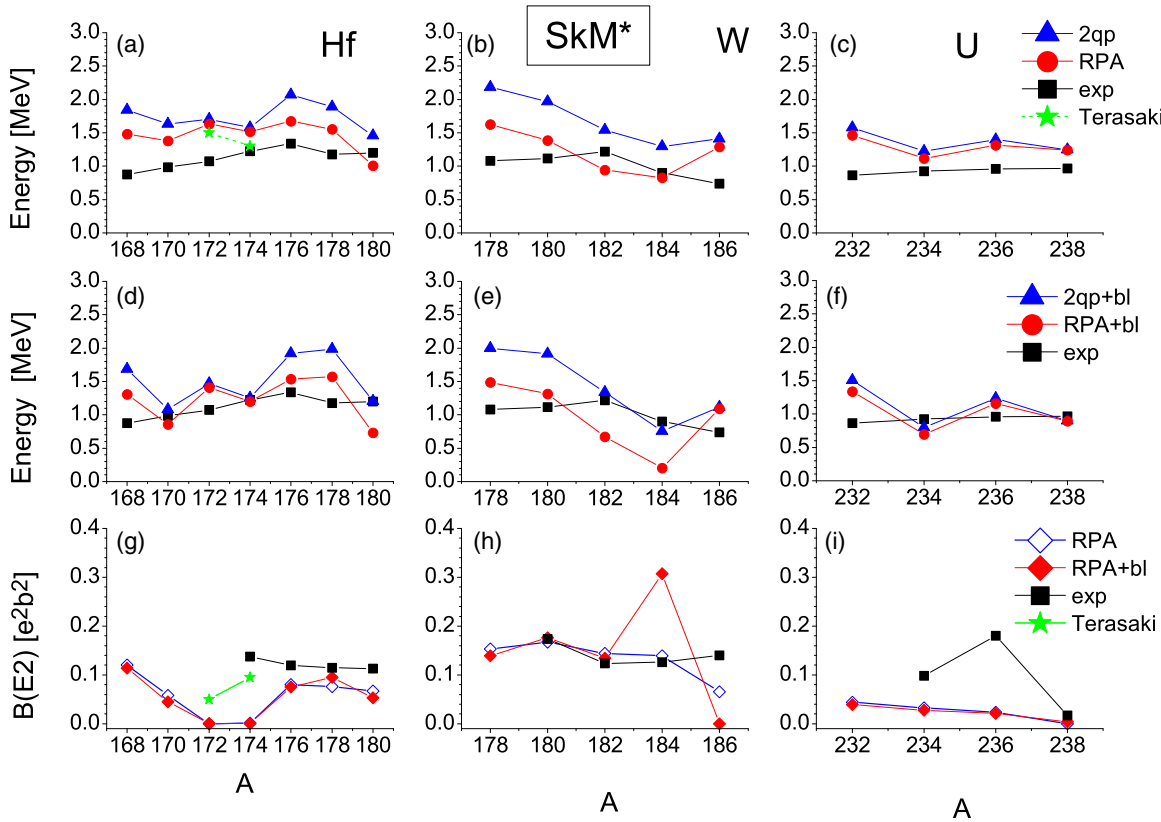

FIG. 10. The same as in Fig. 6 but for the force SkM*.

TABLE I. Deviations between the calculated and experimental values of 2^+_γ energies (σ_E) and $B(E2)$ strengths (σ_B). $\mathcal{N}_{E,B}$ is the number of the involved nuclei. The SRPA deviations are compared with ones from [10].

	Skyrme force	$\mathcal{N}_E$	σ_E (MeV)		$\mathcal{N}_B$	σ_B (e^2b^2)	
			no PBE	PBE		no PBE	PBE
SRPA	SV-bas	40	0.87	0.62	31	0.046	0.056
	SkM*	40	0.52	0.40[a]	31	0.059	0.075[a]
	SkM*	24	0.52	0.44[a]	18	0.061	0.078[a]
Ref. [10]	SkM*	24	0.49		18	0.034	

[a]In SkM* SRPA (PBE) estimation for $\sigma_{E,B}$, the anomalous nucleus ^{164}Dy is omitted [$\mathcal{N}_E = 39(23)$ and $\mathcal{N}_B = 30(17)$].

where $b_i^{\rm cal}$ and $b_i^{\rm exp}$ are calculated and experimental values and $\mathcal{N}_b$ is the number of involved nuclei. The deviations for the SRPA energies (σ_E) and $B(E2)$ values (σ_B) are presented in Table I. The cases with and without PBE are estimated. In the lower part of the table, the SkM* SRPA deviations (without blocking) are compared with those of Ref. [10] (manually obtained from the figures of [10]).

Table I confirms that inclusion of PBE significantly improves description of 2^+_γ energies but somewhat worsens reproduction of $B(E2)$. This takes place for both SV-bas and SkM*. In agreement with previous findings, SkM* describes the energies noticeably better than SV-bas. Compared to [10], SRPA demonstrates better (similar) performance for 2^+_γ energies for the cases with (without) PBE. However, SRPA results are generally worse for $B(E2)$. Perhaps the latter is caused by the impact of the pp channel, which is included in [10] but skipped in SRPA.

Following Table I, the performance of both SRPA and HFB+QRPA [10] is generally not good. The deviations $\sigma_{E,B}$ are large. This calls for further improvement of the description, e.g., for inclusion of the coupling to complex configurations (CCC). The calculated QRPA energies of 2^+_γ states mostly overestimate the experimental values. Thus we still have a window for CCC which, being a sort of additional correlations, can in some cases downshift the energies of the lowest excited states.

Note also that the description of 2^+_γ states depends on a fragile balance of many factors (optimal s-p scheme, deformation, pairing with PBE and pp channel, CCC with the corrections from the Pauli principle, etc.) with comparable impacts. Moreover, these ingredients have opposite effects which partly compensate each other (e.g., the corrections from the Pauli principle may suppress the impact of CCC [23]). Then, adding one of the factors, while ignoring its balance by others, may even worsen the description. In this connection, it would be premature to state, for example, that the performance of SV-bas for 2^+_γ states is worse than that of SkM*. Also it would be wrong to state that if the effect of the particular factor is comparable with the dependence on the Skyrme parametrization, then this factor should be skipped. The final conclusions can be made only after collecting all the relevant factors that can affect the result.

B. Discussion

In this subsection, we analyze the above results and compare them with earlier studies [10,21,23,24].

First of all, it is worthwhile to explore the origin of domains with low and high collectivity of 2^+_γ states. The low-collectivity domains include most of Nd, Er, Yb, Hf, and U isotopes. High collectivity exists in Sm, Gd, Dy, and W isotopes. Table II shows that the appearance of such domains is determined by the structure of the first 2qp states which, in turn, results in different absolute values of the matrix element $f_{ij}^{22} = \langle ij|r^2Y_{22}|0\rangle$ for the doorway operator r^2Y_{22}. These 2qp states are built from the s-p states with the energies close to the Fermi level. High collectivity (pertinent to ^{154}Sm, ^{162,164}Dy, ^{176}Hf, and ^{182}W) takes place if the state is characterized by a large value of $|f_{ij}^{22}|$. Instead, if $|f_{ij}^{22}|$ is small, then we get noncollective 2^+_γ states (^{172}Yb and ^{174}Hf). The magnitude of $|f_{ij}^{22}|$ is determined by Nilsson selection rules for $E2(K=2)$ transitions in axial nuclei [22,50]. The rules read

$$\Delta K = 2, \quad \Delta N = 0, \pm 2, \quad \Delta n_z = 0, \quad \Delta\Lambda = 2, \qquad (16)$$

where N is the principle quantum shell number, n_z is the fraction of N along the z axis, and Λ is the orbital momentum projection onto the z axis. All the 2qp states in Table II fulfill the rules (16) for K and N but not for n_z and Λ. Table II shows that the rule $\Delta n_z = 0$ is decisive. The 2qp states which keep this rule (^{154}Sm, ^{162,164}Dy, ^{176}Hf, ^{182}W) exhibit $|f_{ij}^{22}|$ values one order of magnitude larger than states violating the rule (^{172}Yb and ^{174}Hf). This effect is especially spectacular for neighboring isotopes ^{174}Hf – ^{176}Hf. The rule $\Delta\Lambda = 2$ is not so crucial. However, matrix elements are additionally increased if this rule is obeyed (^{176}Hf, ^{182}W).

Table II obviously suggests that just the strength $|f_{ij}^{22}|$ of the first 2qp state is decisive for the collectivity of the QRPA 2^+_γ state and formation of domains with low and high collectivity. This finding can be corroborated within a simple two-pole model given in Appendix C. Following this model, the collectivity of the lowest QRPA states is mainly determined by the ratio between the strengths of the first ($\nu = 1$) and second ($\nu = 2$) 2qp states where the second state simulates a cumulative effect of all 2qp states with $\nu > 1$. Depending on this ratio, different scenarios can take place: high-collective limit, intermediate case, and low-collective limit. In the last case, the first QRPA energy can lie even a bit above the energy of the first 2qp state, which happens, e.g., in our calculations for Yb isotopes.

Altogether, we get a simple recipe for predicting the collectivity of the first QRPA state: it suffices to inspect the Nilsson selection rules (16) for the lowest 2qp state, first of all $\Delta n_z = 0$. Note that, unlike s-p spectra, the s-p wave functions and thus the values $|f_{ij}^{22}|$ only slightly depend on the Skyrme parametrization [51], which makes the proposed recipe quite reliable. As seen from Table II, SV-bas and SkM* sometimes give different lowest 2qp states. Nonetheless, the correlation between $\Delta n_z = 0$ rule and collectivity of QRPA 2^+_γ states applies in all considered cases.

The nucleus ^{164}Dy computed with SkM* shows a remarkable sequence of four strong ($|f_{ij}^{22}| = 5.8$–9.2 fm^4) 2qp states which are located with PBE at 0.86–1.96 MeV. The cumulative

TABLE II. Features of the lowest (after blocking) 2qp (ij) and corresponding $\lambda\mu\nu = 221$ SRPA states in rare-earth nuclei, calculated with SV-bas and SkM* forces. The table includes the notation $qq[Nn_z\Lambda]_i[Nn_z\Lambda]_j$ of 2qp state in Nilsson quantum numbers; location of the s-p levels i and j relative to the Fermi (F) level; the quadrupole 2qp matrix element $f_{ij}^{22} = \langle ij|r^2Y_{22}|0\rangle$; the 2qp energy ϵ_{ij}^q (5) and collective shift $\Delta E = \epsilon_{ij}^q - E_{221}$, calculated without the blocking; the 2qp energy $\mathcal{E}_{\rm bl}^q(ij)$ (12) and collective shift $\Delta E_{\rm bl} = \mathcal{E}_{\rm bl}^q(ij) - E_{221}$, calculated with the blocking; and the blocking correction $\Delta\mathcal{E}_{\rm bl}^q = \epsilon_{ij}^q - \mathcal{E}_{\rm bl}^q(ij)$. See text for more details.

Nucleus	Force	$qq[Nn_z\Lambda]_i[Nn_z\Lambda]_j$	F location	f_{ij}^{22} (fm^4)	ϵ_{ij}^q (MeV)	ΔE (MeV)	$\mathcal{E}_{\rm bl}^q(ij)$ (MeV)	$\Delta E_{\rm bl}$ (MeV)	$\Delta\mathcal{E}_{\rm bl}^q$ (MeV)
$^{154}_{62}$Sm$_{92}$	SV-bas	$pp[413]\downarrow[411]\downarrow$	F, F+3	−4.43	2.57	0.46	2.34	0.38	0.23
	SkM*	$pp[411]\downarrow[411]\uparrow$	F+3, F+1	4.98	2.45	0.34	2.37	0.31	0.07
$^{162}_{66}$Dy$_{96}$	SV-bas	$pp[411]\downarrow[411]\uparrow$	F+1, F	6.58	1.92	0.65	1.39	0.65	0.53
	SkM*	$pp[413]\downarrow[411]\downarrow$	F, F+1	−5.78	1.71	0.87	1.37	0.88	0.33
$^{164}_{66}$Dy$_{98}$	SV-bas	$pp[411]\downarrow[411]\uparrow$	F+1, F	6.59	1.86	0.57	1.34	0.59	0.51
	SkM*	$nn[523]\downarrow[521]\downarrow$	F, F+1	5.98	1.42	0.56	0.86	0.86	0.56
$^{172}_{70}$Yb$_{102}$	SV-bas	$nn[512]\uparrow[521]\downarrow$	F+1, F − 1	0.37	2.40	0.003	2.12	−0.02	0.28
	SkM*	$nn[512]\uparrow[521]\downarrow$	F+1, F − 1	0.086	1.63	0.06	1.30	0.06	0.33
$^{174}_{72}$Hf$_{102}$	SV-bas	$nn[512]\uparrow[521]\downarrow$	F+1, F − 1	0.37	2.39	−0.02	2.07	0.05	0.32
	SkM*	$nn[512]\uparrow[521]\downarrow$	F+1, F − 1	0.19	1.58	0.06	1.26	0.06	0.33
$^{176}_{72}$Hf$_{104}$	SV-bas	$nn[512]\uparrow[510]\uparrow$	F, F−2	−8.17	2.48	0.47	2.14	0.34	0.33
	SkM*	$nn[512]\uparrow[510]\uparrow$	F, F−2	−8.48	2.53	0.51	2.23	0.39	0.31
$^{182}_{74}$W$_{108}$	SV-bas	$nn[510]\uparrow[512]\downarrow$	F+1, F+2	8.82	2.10	0.68	1.72	0.59	0.39
	SkM*	$nn[510]\uparrow[512]\downarrow$	F+1, F+2	7.98	1.54	0.60	1.34	0.67	0.21

impact of these states delivers a dramatic effect: a breakdown of RPA. Without PBE, these four 2qp states lie at a higher energy, 1.42–2.15 MeV, and do not lead to the instability. For comparison, SV-bas gives in ^{164}Dy only three strong ($|f_{ij}^{22}| = 5.4$–6.6 fm^4) 2qp states, and they are located at a higher energy, 1.35–1.65 MeV. This gives a collective 2_γ^+ state still within QRPA. Altogether, this discussion shows that some QRPA results for low lying states can be quite sensitive to the Skyrme force.

Table II shows that the values of collective shifts ΔE (up to 0.9 MeV) and blocking induced shifts $\Delta\mathcal{E}_{\rm bl}$ (up to 0.6 MeV) are comparable. Thus the PBE has a non-negligible effect in the present calculations.

The results exhibited in Figs. 5–10 indicate that the present Skyrme QRPA description of 2_γ^+ states is not yet fully satisfactory. Though we get rather good agreement with experimental data for collective 2_γ^+ states in Gd, Dy, and W isotopes, collectivity is generally underestimated in other isotopic chains (which is seen from too high SRPA energies and significantly low $B(E2)$ values). Perhaps the latter cases require a coupling to complex configurations, which might affect both the 2_γ^+ energies and $B(E2)$ values. In this respect, our calculations indicate regions where CCC is needed. In the previous Skyrme QRPA study [10], the need for CCC was also pointed out. In nuclei like ^{164}Dy, an approach taking into account large ground state correlations is necessary [47,48].

As seen in Figs. 5–10, the performances of our and previous [10] systematic Skyrme QRPA calculations (without the PBE) are rather similar. Although these calculations exploit different prescriptions, HFB + exact QRPA in [10] and BCS+PBE + separable QRPA in the present study, they provide a remarkably similar description of QRPA energies of 2_γ^+ states. The results [10] are somewhat better for $B(E2)$ values, though the difference is not crucial.

Since SRPA operates with the residual interaction in a separable form, it can be directly compared with schematic separable QRPA approaches, e.g., with QPM, which is widely and successfully used in nuclear spectroscopy [22]. The QPM proposes some simple relations for the strength constants of the residual interaction which might be useful for a rough evaluation of the SRPA strength constants. This analysis is done in Appendix C. It is shown that the mixed isoscalar-isovector interaction might be essential in Skyrme QRPA. If this interaction is not properly balanced, it can weaken a general isoscalar effect of the residual interaction and thus make 2_γ^+ states less collective (which might be relevant for Nd, Yb, Hf, and U isotopes).

IV. SUMMARY

We have performed a systematic study of the lowest γ-vibrational $K^\pi = 2^+$ states in axially deformed even-even rare-earth and actinide nuclei within a self-consistent (except for the pairing part) separable random-phase approximation (SRPA) [5]. Nine isotopic chains involving 41 nuclei were explored. The excitation energies and $B(E2)$ values of 2_γ^+ states were computed and analyzed. The Skyrme forces SV-bas [27] and SkM* [25] were used. The force SV-bas was chosen since it provides a good description of ground state deformations and isoscalar giant quadrupole resonance (ISGQR). SkM* was used as a force with the best performance in the previous systematic study of 2_γ^+ states [10], performed within the exact (not factorized) Skyrme HFB+QRPA. The accuracy of SRPA was confirmed by comparison with calculations within exact BCS+QRPA [39] and HFB+QRPA [10].

Our study undertakes some important steps that were not realized earlier [10]. Some essential points concerning the pairing contribution, systematics of 2_γ^+ states, and explanation of the results were scrutinized.

First, we have investigated a possible impact of the pairing blocking effect (PBE) on the properties of 2^+_γ states. Thereby we use in an *ad hoc* manner only the PBE-corrected 2qp energies, while the 2qp wave functions remain the same as in the BCS ground state. This scheme has significant advantages: it incorporates the most essential energy correction from PBE but maintains, at the same time, the orthonormality of the 2qp configuration space, which, in turn, allows us to apply the standard QRPA solution scheme. The scheme was applied to a few lowest two-quasiparticle (2qp) configurations whose corrected energies were then used in SRPA calculations. In this framework, the PBE significantly downshifts the SRPA energies of 2^+_γ states and thus improves agreement with the experimental spectra. At the same time, PBE rather slightly affects collectivity of the states, expressed in terms of collective shifts and transition probabilities $B(E2)$. Note that our present handling of the PBE is very preliminary and should be further checked in a fully developed self-consistent QRPA with PBE. To the best of our knowledge, such methods are still absent. Then our study can be viewed as a first step which highlights the problem and calls for a further self-consistent exploration. Note also that the PBE-QRPA scheme is certainly not the only way to improve the description of 2^+_γ states. Various many-body techniques that go beyond the plain QRPA, first of all the coupling to complex configuration, can be decisive here.

As the next novel aspect of our study, we have singled out domains of nuclei with low and high collectivity of 2^+_γ states. It was shown that collectivity is mostly determined by the structure of the lowest 2qp state dominating the first SRPA state. The effect was explained in terms of the Nilsson selection rule $\Delta n_z = 0$, which delivers a simple recipe to predict the 2^+_γ collectivity without performing QRPA calculations. Some SRPA characteristics were compared with those from the schematic quasiparticle-phonon model (QPM) [22] which was successfully used for a long time in nuclear spectroscopy.

It was found that the forces SV-bas and SkM* perform similarly in the description of 2^+_γ states for light rare-earth nuclei but deviate in heavier nuclei. The latter is mainly explained by the fact that SkM* delivers a weaker pairing gap and thus lower 2qp energies than SV-bas. SV-bas delivers less fluctuating trends of energies and $B(E2)$ values, and well describes Dy isotopes but fails in U isotopes. SkM* is better in U isotopes but its results fluctuate more with the mass number. Moreover, SV-bas has an important advantage over SkM*: it well describes quadrupole equilibrium deformations and energy centroids of ISGQR. Thus SV-bas allows us to get a consistent description of 2^+_γ states and ISGQR.

In general our study shows that, despite all the progress, available fully or partly self-consistent QRPA schemes are still not accurate enough for a satisfactory description of 2^+_γ states throughout medium and heavy axially deformed nuclei. This holds for both our results and previous ones [10]. Some essential factors should be still added or improved. The proper calculation scheme should fulfill at least the following requirements: (a) accurate description of the s-p spectra and equilibrium deformation, (b) treatment of pairing (BCS or HFB) with PBE, (c) self-consistent residual QRPA interaction with both *ph* and *pp* channels and consistently incorporated PBE, (d) simultaneous description of other quadrupole excitations (ISGQR), (e) systematic description involving nuclei from various mass regions and domains with low and high collectivity, and (f) the coupling to complex configuration (with the proper inclusion of the Pauli principle). Some of these points will be subjects of our next studies.

ACKNOWLEDGMENTS

The work was partly supported by the DFG grant RE 322/14-1, Heisenberg-Landau (Germany-BLTP JINR), and Votruba-Blokhintsev (Czech Republic-BLTP JINR) grants. BMBF support under the contracts 05P12RFFTG (P.-G.R.) and 05P12ODDUE (W.K.) is appreciated. J.K. is grateful for support of the Czech Science Foundation (P203-13-07117S). We thank J. Terasaki, A.V. Sushkov, and A. P. Severyukhin for useful discussions.

APPENDIX A: PAIRING CUTOFF WEIGHT AND PAIRING MATRIX ELEMENTS

To simulate the effect of a finite range pairing force, the pairing-active space for each isospin q is limited by using a smooth energy-dependent cutoff (see, e.g., [33,52])

$$f^q_k = \frac{1}{1+\exp\left[\frac{\tilde{e}^q_k-\lambda_q-\Delta E_q}{\eta_q}\right]} \tag{A1}$$

in the sums in Eqs. (9), (10), (13), and (14). The cutoff parameters ΔE_q and $\eta_q = \Delta E_q/10$ are chosen to be self-adjusting to the actual level density in the vicinity of the Fermi energy; see [34] for details.

For the δ-force pairing interaction (3), the antisymmetrized pairing matrix elements read

$$\begin{aligned} V^{(\mathrm{pair,q})}_{i\bar{i}\,j\bar{j}} &= \langle i\bar{i}|V^q_{\mathrm{pair}}(\mathbf{r},\mathbf{r}')|j\bar{j}\rangle_q \\ &= \int d^3r \int d\mathbf{r}'\, \Phi^+_i(\mathbf{r})\Phi^+_{\bar{i}}(\mathbf{r}')\, V_q\, \delta(\mathbf{r}-\mathbf{r}') \\ &\quad \cdot[\Phi_j(\mathbf{r})\Phi_{\bar{j}}(\mathbf{r}') - \Phi_j(\mathbf{r}')\Phi_{\bar{j}}(\mathbf{r})] \\ &= V_q \int d^3r[(\Phi^+_i(\mathbf{r})\cdot\Phi_j(\mathbf{r}))(\Phi^+_{\bar{i}}(\mathbf{r})\cdot\Phi_{\bar{j}}(\mathbf{r})) \\ &\quad -(\Phi^+_i(\mathbf{r})\cdot\Phi_{\bar{j}}(\mathbf{r}))(\Phi^+_{\bar{i}}(\mathbf{r})\cdot\Phi_j(\mathbf{r}))], \end{aligned} \tag{A2}$$

where

$$\Phi_i(\mathbf{r}) = \begin{pmatrix} R^{(+)}_i(\rho,z)\; e^{i(K_i-\frac{1}{2})\vartheta} \\ R^{(-)}_i(\rho,z)\; e^{i(K_i+\frac{1}{2})\vartheta} \end{pmatrix}, \tag{A3}$$

$$\Phi_{\bar{i}}(\mathbf{r}) = \begin{pmatrix} -R^{(-)}_i(\rho,z)\; e^{-i(K_i+\frac{1}{2})\vartheta} \\ R^{(+)}_i(\rho,z)\; e^{-i(K_i-\frac{1}{2})\vartheta} \end{pmatrix} \tag{A4}$$

are spinor s-p wave functions in cylindrical coordinates (ρ,z,ϑ) and $(\Phi_i^+(\mathbf{r})\cdot\Phi_j(\mathbf{r}))$ are scalar products. Denoting the first (Hartree) and second (exchange) terms in the last line of (A2) as $V_{i\bar{i}j\bar{j}}^{(\text{pair}-\text{H,q})}$ and $V_{i\bar{i}j\bar{j}}^{(\text{pair}-\text{ex,q})}$, we obtain

$$V_{i\bar{i}j\bar{j}}^{(\text{pair-H,q})} = 2\pi\, V_q \int_0^\infty d\rho \int_{-\infty}^\infty dz\, \rho\big[2R_i^{(+)}R_j^{(+)}R_i^{(-)}R_j^{(-)} + \big(R_i^{(-)}R_j^{(-)}\big)^2 + \big(R_i^{(+)}R_j^{(+)}\big)^2\big], \tag{A5}$$

$$V_{i\bar{i}j\bar{j}}^{(\text{pair-ex,q})} = 2\pi\, V_q \int_0^\infty d\rho \int_{-\infty}^\infty dz\, \rho\big[-2R_i^{(+)}R_j^{(-)}R_i^{(-)}R_j^{(+)} + \big(R_i^{(+)}R_j^{(-)}\big)^2 + \big(R_i^{(-)}R_j^{(+)}\big)^2\big], \tag{A6}$$

and finally

$$\begin{aligned} V_{i\bar{i}j\bar{j}}^{(\text{pair,q})} &= V_{i\bar{i}j\bar{j}}^{(\text{pair-H,q})} + V_{i\bar{i}j\bar{j}}^{(\text{pair-ex,q})} \\ &= 2\pi\, V_q \int_0^\infty d\rho \int_{-\infty}^\infty dz\, \rho\big[\big[\big(R_i^{(+)}\big)^2 + \big(R_i^{(-)}\big)^2\big]\big[\big(R_j^{(+)}\big)^2 + \big(R_j^{(-)}\big)^2\big]\big]. \end{aligned} \tag{A7}$$

APPENDIX B: BASIC SRPA EQUATIONS

The self-consistent derivation [5,38] yields the SRPA Hamiltonian

$$\hat{H} = \sum_q \hat{h}_{\text{HF+BCS}}^q + \hat{V}_{\text{res}}, \tag{B1}$$

where

$$\hat{h}_{\text{HFB}}^q = \int d\mathbf{r} \sum_{\alpha,\alpha'} \left[\frac{\delta E}{\delta J_\alpha^q(\mathbf{r})}\hat{J}_\alpha^q(\mathbf{r})\right] \tag{B2}$$

is the mean field and pairing contribution and

$$\hat{V}_{\text{res}} = -\frac{1}{2}\sum_{qq'}\sum_{m,m=1}^{M}[\kappa_{qm,q'm'}\hat{X}_{qm}\hat{X}_{q'm'} + \eta_{qm,q'm'}\hat{Y}_{qm}\hat{Y}_{q'm'}] \tag{B3}$$

is the separable residual interaction with one-body operators

$$\begin{aligned} \hat{X}_{qm} = \sum_{q'}\hat{X}_{qm}^{q'} &= i\sum_{q'}\sum_{\alpha,\alpha'}\int d\mathbf{r}\left[\frac{\delta^2 E}{\delta J_{\alpha'}^{q'}(\mathbf{r}')\delta J_\alpha^q(\mathbf{r})}\right] \\ &\times\big\langle\big[\hat{P}_{qm},\hat{J}_\alpha^q(\mathbf{r})\big]\big\rangle\hat{J}_{\alpha'}^{q'}(\mathbf{r}'), \end{aligned} \tag{B4}$$

$$\begin{aligned} \hat{Y}_{qm} = \sum_{q'}\hat{Y}_{qm}^{q'} &= i\sum_{q'}\sum_{\alpha,\alpha'}\int d\mathbf{r}\left[\frac{\delta^2 E}{\delta J_{\alpha'}^{q'}(\mathbf{r}')\delta J_\alpha^q(\mathbf{r})}\right] \\ &\times\big\langle\big[\hat{Q}_{qm},\hat{J}_\alpha^q(\mathbf{r})\big]\big\rangle\hat{J}_{\alpha'}^{q'}(\mathbf{r}') \end{aligned} \tag{B5}$$

and inverse strength matrices

$$\kappa_{qmq'm'}^{-1} = -i\langle[\hat{P}_{qm},\hat{X}_{q'm'}]\rangle, \tag{B6}$$

$$\eta_{qmq'm'}^{-1} = -i\langle[\hat{Q}_{qm},\hat{Y}_{q'm'}]\rangle. \tag{B7}$$

Here $\alpha = \rho,\tau,\mathbf{J},\chi,\mathbf{j},\mathbf{s},\mathbf{T}$ enumerates densities J_α^q and their operators $\hat{J}_\alpha^q$ while m marks time-even $\hat{Q}_{qm}$ and time-odd $\hat{P}_{qm} = i[\hat{H},\hat{Q}_{qm}]$ Hermitian input (doorway) operators. The number M of separable terms in (B3) is determined by the number of the input operators $\hat{Q}_{qm}$ chosen from physical arguments [5,37]. Usually we have $M = 3$–5. For such cases, the SRPA matrix has a low rank, $4M$, and we have small computational expense even for heavy deformed nuclei.

The values $\langle[\hat{P}_{qm},\hat{J}_\alpha^q]\rangle$ from (B4) and $\langle[\hat{Q}_{qm},\hat{J}_\alpha^q]\rangle$ from (B5) do not vanish only for time-even and time-odd densities $\hat{J}_\alpha^q$, respectively. Then $\hat{X}_k$ is time-even (determined by time-even densities) while $\hat{Y}_k$ is time-odd (determined by time-odd densities). The SRPA residual interaction (B3) includes contributions from variations of both time-odd and time-even densities.

Following (B2), (B4), and (B5), $\hat{h}_{\text{HF+BCS}}$ and $\hat{V}_{\text{res}}$ are determined by first and second functional derivatives of the given energy functional. The model is self-consistent with the exception of the pairing part.

The operators $\hat{Q}_{qm}$ constitute the key input for SRPA [5,37]. They are chosen from physical arguments, namely to produce doorway states for particular excitations. In the present calculations, four operators are used. The first one, $\hat{Q}_{q1}(\mathbf{r}) = r^2Y_{22}(\theta) + \text{h.c.}$, generates the quadrupole ($\lambda\mu = 22$) mode of interest in the long-wave approximation ($Y_{22}(\theta)$ is the spherical harmonic). Usually, just one such operator (generator) is enough for a rough description of the spectrum. However the corresponding Tassie mode [31,53] is mainly of surface character. So, to improve accuracy of the description, two other generators, $\hat{Q}_{q2}(\mathbf{r}) = r^4Y_{22}(\theta) + \text{h.c.}$ and $\hat{Q}_{q3}(\mathbf{r}) = j_2(0.6r)Y_{22}(\theta) + \text{h.c.}$ (with $j_2(0.6r)$ being the spherical Bessel function), are added. These generators result in $\hat{X}_{qm}^{q'}(\mathbf{r})$ operators peaked more in the nuclear interior [5]. Finally, the generator $\hat{Q}_{q4}(\mathbf{r}) = r^4Y_{42}(\theta) + \text{h.c.}$ is added to take into account the coupling between quadrupole and hexadecapole excitations in axially deformed nuclei. Note that these input operators do not form directly the separable residual interaction (B3) but generate its operators $\hat{X}_{qm}^{q'}(\mathbf{r})$, $\hat{Y}_{qm}^{q'}(\mathbf{r})$ and strength constants $\kappa_{qm,q'm'}$, $\eta_{qm,q'm'}$, based on the initial Skyrme functional. The number M of input operators determines the number of the separable terms in (B3). Larger M brings the separable interaction closer to the true (not factorized) one, but makes SRPA calculations more time consuming. The four operators which we are using here constitute a good compromise between reliability and expense.

SRPA allows us to calculate the energies ω_ν and wave function (with forward ψ_{ij}^ν and backward ϕ_{ij}^ν 2qp amplitudes) of one-phonon ν states. Besides, various strength functions can be directly computed (without calculation of ν states). In this study, we use for description of ISGQR the strength function

$$S_\gamma(E22,E) = \sum_\nu |\langle\nu|\, r^2Y_{22}\,|0\rangle|^2\,\xi_\Delta(E-E_\nu), \tag{B8}$$

where $\xi_\Delta(E-E_\nu)=\Delta/[2\pi(E-E_\nu)^2+(\Delta/2)^2]$ is the Lorentz weight with the averaging parameter $\Delta=1$ MeV.

The energy centroids for ISGQR depicted in Fig. 3 are estimated for the energy intervals where the strength functions exceeds 20% of its maximal value.

APPENDIX C: SIMPLE TWO-POLE RPA MODEL

Let us consider SRPA with one input (doorway) operator and without time-odd contributions. Then the SRPA secular equation is reduced to the familiar equation for the schematic separable RPA [22,31]:

$$\kappa^{-1}=\sum_{ij}\frac{f_{ij}^2}{\epsilon_{ij}^2-E_\nu^2}, \tag{C1}$$

where κ is the strength constant, f_{ij} is the matrix element of the residual interaction (including the pairing factors) between the states i and j, ϵ_{ij} is the 2qp energy, and E_ν is the energy of the νth RPA state. This equation may be simplified to the case of two 2qp states, yielding two poles in the schematic RPA equation:

$$1=\kappa f^2\left[\frac{k^2}{\epsilon_1^2-E^2}+\frac{1}{\epsilon_2^2-E^2}\right]. \tag{C2}$$

Here the first pole is characterized by the 2qp energy ϵ_1 and matrix element kf. The second pole (with the 2qp energy $\epsilon_2>\epsilon_1$ and matrix element f) is assumed to simulate the effect of all the poles above the lowest one. The coefficient k determines the ratio between the matrix elements of the first and second poles. We suppose $\kappa>0$, which is common for low-energy isoscalar excitations [22].

Equation (C2) is reduced to a standard quadratic equation

$$E^4+bE^2+c=0 \tag{C3}$$

with

$$b=-\left(\epsilon_1^2+\epsilon_2^2\right)+\kappa f^2(1+k^2), \tag{C4}$$

$$c=\epsilon_1^2\epsilon_2^2-\kappa f^2\left(\epsilon_1^2+k^2\epsilon_2^2\right). \tag{C5}$$

This equation allows us to get useful analytical estimations for three important cases: (i) $k\gg1$ (strong first pole, typical for Gd, Dy, and W isotopes), (ii) $k\ll1$ (weak first pole, typical for Nd, Yb, Hf, and U isotopes), and (iii) $k=1$ (intermediate case with equal strengths of the first and second poles).

We go through these three cases step by step:

(i) For the strong first pole ($k\gg1$), we get $(1\pm k^2)\to\pm k^2$ and so

$$E^2\approx\tfrac{1}{2}\left[\epsilon_1^2+\epsilon_2^2-\kappa(fk)^2\pm\left(\epsilon_1^2-\epsilon_2^2-\kappa(fk)^2\right)\right] \tag{C6}$$

with two solutions,

$$E_+^2\approx\epsilon_1^2-\kappa(fk)^2,\quad E_-^2\approx\epsilon_2^2. \tag{C7}$$

The solution E_+ gives the energy of the first RPA state below the first pole, which is a common case in phenomenological QPM [21–23]. In our calculations, this case is met in Gd, Dy, and W isotopes.

(ii) For the weak first pole ($k\ll1$), we get $(1\pm k^2)\to1$, and so

$$E^2\approx\tfrac{1}{2}\left[\epsilon_1^2+\epsilon_2^2-\kappa f^2\pm\left(\epsilon_1^2-\epsilon_2^2+\kappa f^2\right)\right], \tag{C8}$$

$$E_+^2\approx\epsilon_1^2,\quad E_-^2\approx\epsilon_2^2-\kappa f^2. \tag{C9}$$

The solution E_+ is the energy of the first RPA state close to the first pole. This energy can be both a bit smaller or larger than e_1. We have this case for Nd, Yb, and Hf isotopes.

(iii) If the pole strengths are equal ($k=1$), then $(1-k^2)\to0$, $(1+k^2)\to2$, and

$$E^2\approx\tfrac{1}{2}\left[\epsilon_1^2+\epsilon_2^2-2\kappa f^2\pm\sqrt{\left(\epsilon_1^2-\epsilon_2^2\right)^2+4\kappa^2f^4}\right]. \tag{C10}$$

Supposing that $(\epsilon_1^2-\epsilon_2^2)^2\gg4\kappa^2f^4$, we get

$$E^2\approx\tfrac{1}{2}\left[\epsilon_1^2+\epsilon_2^2-2\kappa f^2\pm\left(\epsilon_1^2-\epsilon_2^2+\kappa f^2\right)\right], \tag{C11}$$

$$E_+^2\approx\epsilon_1^2-\tfrac{1}{2}\kappa f^2,\quad E_-^2\approx\epsilon_2^2-\tfrac{3}{2}\kappa f^2. \tag{C12}$$

This simple model indicates that collectivity (collective shift $\Delta E=E_+-\epsilon_1$) of the first RPA state is determined to a large extent by the relative strength of the first pole. This conclusion is confirmed by our numerical results; see the discussion of Table II. Thus we have found a simple way for the prediction of the collectivity (weak or large) of the first RPA state. In practice, it is enough to compare the matrix elements of the first and next poles. Or, more easily, one should check if the first pole fulfills the $\Delta n_z=0$ Nilsson selection rule.

APPENDIX D: COMPARISON WITH QPM

Since SRPA deals with a separable residual interaction, this method can be directly compared with the schematic separable QRPA exploited in QPM [22]. The QPM is not self-consistent: it uses the Woods-Saxon s-p basis, and its isoscalar κ_{00} and isovector κ_{11} strength constants of the residual interaction are adjusted to reproduce the experimental energies of lowest vibrational states and giant resonances. However, just because of the successful combination of the microscopic and phenomenological aspects, the QPM is known to be quite accurate in description of low-energy states. Thus it is instructive to compare the characteristics of self-consistent models, like Skyrme QRPA, with the relevant QPM parameters.

In this connection, let us briefly discuss the QPM strength constants of the residual interaction and compare them with the SRPA ones. The strength constants in the proton-neutron domain (nn, pp, np) can be related to their counterparts in the isoscalar-isovector domain (00,11, 01) as

$$\kappa_{00}=\frac{1}{2}(\kappa_{pp}+\kappa_{pn}+\kappa_{np}+\kappa_{nn}), \tag{D1}$$

$$\kappa_{11}=\frac{1}{2}(\kappa_{pp}-\kappa_{pn}-\kappa_{np}+\kappa_{nn}), \tag{D2}$$

$$\kappa_{01}=\frac{1}{2}(\kappa_{pp}-\kappa_{pn}+\kappa_{np}-\kappa_{nn})=\kappa_{10}. \tag{D3}$$

The constants $\kappa_{01} = \kappa_{10}$ represent the mixing between isoscalar (00) and isovector (11) excitations. This mixing can be motivated by both physical (Coulomb interaction, etc.) and technical (different sizes of neutron and proton s-p basis, etc.) reasons. Since nuclei roughly keep the isospin symmetry, then

$$|\kappa_{00}|, |\kappa_{11}| \gg |\kappa_{01} = \kappa_{10}|. \tag{D4}$$

If we assume $\kappa_{01} = \kappa_{10} = 0$ and $\kappa_{np} = \kappa_{pn}$, then we get

$$\kappa_{pp} = \kappa_{nn} \tag{D5}$$

and the familiar QPM relations [22]

$$\kappa_{00} = \kappa_{pp} + \kappa_{pn}, \quad \kappa_{11} = \kappa_{pp} - \kappa_{pn}. \tag{D6}$$

From (D6) one gets

$$\kappa_{pp} = \kappa_{nn} = \tfrac{1}{2}(\kappa_{00} + \kappa_{11}), \tag{D7}$$

$$\kappa_{pn} = \kappa_{np} = \tfrac{1}{2}(\kappa_{00} - \kappa_{11}) \tag{D8}$$

where $\kappa_{11} = \alpha\kappa_{00}$ with $\kappa_{00} > 0$. Usually $\alpha = -1.5$ is used [23], which results in a dominance of the np interaction, $\kappa_{pn}/\kappa_{pp} = -2.5$ with $\kappa_{pn} = \kappa_{np} > 0$ and $\kappa_{pp} = \kappa_{nn} < 0$.

For the comparison, the self-consistent SRPA calculations give a somewhat different picture. As a relevant example, the strength constants $\kappa_{q1,q'1} = \kappa_{qq'}$ for the dominant first input operator r^2Y_{22} in ^{162}Dy are considered. Note that in SRPA the relation $\kappa_{pn} = \kappa_{np}$ is kept. SV-bas gives strength constants $\kappa_{pp}, \kappa_{nn}, \kappa_{pn} > 0$ with the relations $\kappa_{pp}/\kappa_{nn} = 2.7$, $\kappa_{pn}/\kappa_{pp} = 7.7$, and $\kappa_{pn}/\kappa_{nn} = 2.9$. Similar results are obtained in other nuclei. SkM* gives $\kappa_{nn}, \kappa_{pn} > 0$, $\kappa_{pp} < 0$ and relations $\kappa_{pp}/\kappa_{nn} = -2.0$, $\kappa_{pn}/\kappa_{pp} = -4.4$, and $\kappa_{pn}/\kappa_{nn} = 2.2$. In agreement with QPM, both forces provide a dominant np interaction with the proper sign. However, in contrast to (D5), the weak SRPA constants κ_{pp} and κ_{nn} noticeably deviate from each other, which might be a signature of a large mixing of the isoscalar and isovector interaction. Perhaps just this mixing, if not be properly balanced with other parts of the interaction, partly leads to the troubles of Skyrme QRPA with the description of 2^+_γ states. A difference in sign of SV-bas and SkM* constants κ_{pp} should be also mentioned as demonstration of the noticeable dependence of the residual interaction on the Skyrme force.

[1] M. Bender, P.-H. Heenen, and P.-G. Reinhard, Rev. Mod. Phys. **75**, 121 (2003).
[2] D. Vretenar, A. V. Afanasjev, G. A. Lalazissis, and P. Ring, Phys. Rep. **409**, 101 (2005).
[3] N. Paar, D. Vretenar, E. Khan, and G. Colo, Rep. Prog. Phys. **70**, 691 (2007).
[4] J. Erler, W. Kleinig, P. Klüpfel, J. Kvasil, V. O. Nesterenko, and P.-G. Reinhard, Phys. Part. Nucl. **41**, 851 (2010).
[5] V. O. Nesterenko, W. Kleinig, J. Kvasil, P. Vesely, P.-G. Reinhard, and D. S. Dolci, Phys. Rev. C **74**, 064306 (2006).
[6] K. Yoshida and N. V. Giai, Phys. Rev. C **78**, 064316 (2008).
[7] D. Pena Arteaga and P. Ring, Phys. Rev. C **77**, 034317 (2008).
[8] C. Losa, A. Pastore, T. Døssing, E. Vigezzi, and R. A. Broglia, Phys. Rev. C **81**, 064307 (2010).
[9] J. Terasaki and J. Engel, Phys. Rev. C **82**, 034326 (2010).
[10] J. Terasaki and J. Engel, Phys. Rev. C **84**, 014332 (2011).
[11] S. Péru and H. Goutte, Phys. Rev. C **77**, 044313 (2008).
[12] S. Péru, G. Gosselin, M. Martini, M. Dupuis, S. Hilaire, and J.-C. Devaux, Phys. Rev. C **83**, 014314 (2011).
[13] T. Inakura, T. Nakatsukasa, and K. Yabana, Phys. Rev. C **80**, 044301 (2009).
[14] S. Fracasso, E. B. Suckling, and P. D. Stevenson, Phys. Rev. C **86**, 044303 (2012).
[15] N. Hinohara, M. Kortelainen, and W. Nazarewicz, Phys. Rev. C **87**, 064309 (2013).
[16] V. O. Nesterenko, W. Kleinig, J. Kvasil, P. Vesely, and P.-G. Reinhard, Int. J. Mod. Phys. E **17**, 89 (2008).
[17] W. Kleinig, V. O. Nesterenko, J. Kvasil, P.-G. Reinhard, and P. Vesely, Phys. Rev. C **78**, 044313 (2008).
[18] J. Kvasil, V. O. Nesterenko, W. Kleinig, D. Bozik, P.-G. Reinhard, and N. Lo Iudice, Eur. Phys. J. A **49**, 119 (2013).
[19] P. Vesely, J. Kvasil, V. O. Nesterenko, W. Kleinig, P.-G. Reinhard, and V. Yu. Ponomarev, Phys. Rev. C **80**, 031302(R) (2009).
[20] Evaluated Nuclear Structure Data File, http://www.nndc.bnl.gov
[21] E. P. Grigorjev and V. G. Soloviev, *Structure of Even Deformed Nuclei* (Nauka, Moscow, 1974).
[22] V. G. Soloviev, *Theory of Atomic Nuclei* (Pergamon Press, Oxford, 1976).
[23] V. G. Soloviev and N. Yu. Shirikova, Z. Phys. A - Atomic Nuclei **334**, 149 (1989).
[24] V. G. Soloviev, A. V. Sushkov, and N. Yu. Shirikova, Phys. Part. Nucl. **27**, 667 (1996).
[25] J. Bartel, P. Quentin, M. Brack, C. Guet, and H.-B. Haakansson, Nucl. Phys. A **386**, 79 (1982).
[26] E. Chabanat, P. Bonche, P. Haensel, J. Meyer, and R. Schaeffer, Nucl. Phys. A **635**, 231 (1998).
[27] P. Klupfel, P.-G. Reinhard, T. J. Burvenich, and J. A. Maruhn, Phys. Rev. C **79**, 034310 (2009).
[28] V. O. Nesterenko, V. G. Kartavenko, W. Kleinig, R. V. Jolos, J. Kvasil, and P.-G. Reinhard, arXiv:1504.06492 [nucl-th].
[29] K. J. Pototzky, J. Erler, P.-G. Reinhard, and V. O. Nesterenko, Eur. Phys. J. A **46**, 299 (2010).
[30] J. M. Eisenberg and W. Greiner, *Nuclear Theory: Microscopic Theory of the Nucleus*, Vol. III (North-Holland, Amsterdam, 1972).
[31] P. Ring and P. Schuck, *Nuclear Many Body Problem* (Springer-Verlag, New York, 1980).
[32] S. G. Nilsson and I. Ragnarsson, *Shapes and Shells in Nuclear Structure* (Cambridge University Press, Cambridge, 1995).
[33] *Fifty Years of Nuclear BCS*, edited by R. A. Broglia and V. Zelevinsky (World Scientific, Singapore, 2013).
[34] M. Bender, K. Rutz, P.-G. Reinhard, and J. A. Maruhn, Eur. Phys. J. A **8**, 59 (2000).
[35] T. H. R. Skyrme, Philos. Mag. **1**, 1043 (1956).
[36] D. Vauterin and D. M. Brink, Phys. Rev. C **5**, 626 (1972).
[37] V. O. Nesterenko, J. Kvasil, and P.-G. Reinhard, Phys. Rev. C **66**, 044307 (2002).

[38] V. O. Nesterenko, J. Kvasil, W. Kleinig, P.-G. Reinhard, and D. S. Dolci, arXiv:nucl-th/0512045.
[39] A. Repko, J. Kvasil, V. O. Nesterenko, and P.-G. Reinhard, arXiv:1510.01248 [nucl-th].
[40] P.-G. Reinhard (private communication).
[41] S. Raman, C. W. Nestor Jr., and P. Tikkanen, At. Data Nucl. Data Tables **78**, 1 (2001).
[42] T. Duguet, P. Bonche, P.-H. Heenen, and J. Meyer, Phys. Rev. C **65**, 014310 (2001).
[43] N. K. Kuzmenko, V. M. Mikhailov, and V. O. Nesterenko, Bull. Acad. Sci. USSR, Phys. Ser. **50**, 41 (1986).
[44] J. Dobaczewski, M. V. Stoitsov, W. Nazarewicz, and P.-G. Reinhard, Phys. Rev. C **76**, 054315 (2007).
[45] G. Scamps and D. Lacroix, Phys. Rev. C **88**, 044310 (2013).
[46] A. P. Severyukhin, V. V. Voronov, and N. V. Giai, Phys. Rev. C **77**, 024322 (2008).
[47] K. E. Hara, Prog. Theor. Phys. **32**, 88 (1964).
[48] V. V. Voronov, D. Karadjov, F. Catara, and A. P. Severyukhin, Phys. Part. Nucl. **31**, 452 (2000).
[49] P. Klüpfel, J. Erler, P.-G. Reinhard, and J. A. Maruhn, Eur. Phys. J. A **37**, 343 (2008).
[50] B. Mottelson and S. G. Nilsson, Mat. Fys. Skr. Dan. Vid. Selsk **1**, No. 8 (1959).
[51] V. O. Nesterenko, V. P. Likhachev, P.-G. Reinhard, V. V. Pashkevich, W. Kleinig, and J. Mesa, Phys. Rev. C **70**, 057304 (2004).
[52] P. Bonche, H. Flocard, P. H. Heenen, S. J. Krieger, and M. S. Weiss, Nucl. Phys. A **443**, 39 (1985).
[53] L. J. Tassie, Aust. J. Phys. **9**, 407 (1956).